Title

Functionalized polymeric nanoparticles loaded with indocyanine green as theranostic materials for targeted molecular near infrared fluorescence imaging and photothermal destruction of ovarian cancer cells.

Journal

Lasers in surgery and medicine, 46(7)

ISSN

0196-8092

Authors

Bahmani, Baharak
Guerrero, Yadir
Bacon, Danielle
et al.

Publication Date

2014-09-01

DOI

10.1002/lsm.22269

Peer reviewed

Functionalized Polymeric Nanoparticles Loaded with Indocyanine Green as Theranostic Materials for Targeted Molecular Near Infrared Fluorescence Imaging and Photothermal Destruction of Ovarian Cancer Cells

Baharak Bahmani, PhD,[1] Yadir Guerrero, BS,[1] Danielle Bacon,[1] Vikas Kundra, MD, PhD,[2] Valentine I. Vullev, PhD,[1] and Bahman Anvari, PhD[1]*

[1]*Department of Bioengineering, University of California, Riverside, California 92521*

[2]*Department of Diagnostic Radiology, The University of Texas, MD Anderson Cancer Center, Houston, Texas 77030*

Background and Objectives: Ovarian cancer remains the deadliest malignancy of the female reproductive system. The ability to identify and destroy all ovarian tumor nodules may have a termendous impact on preventing tumor recurrence, and patient survival. The objective of this study is to investigate the effectiveness of a nano-structured system for combined near infrared (NIR) fluorescence imaging of human epidermal growth factor receptor-2 (HER2) over-expression, as a biomarker of ovarian cancer cells, and photothermal destruction of these cells *in vitro*.

Materials and Methods: The nano-structured system consists of the near infrared dye, indocyanine green (ICG), encapsulated within poly(allylamine) hydrochloride chains cross-linked ionically with sodium phosphate. The surface of the construct is functionalized by covalently attached polyethylene glycol, and monoclonal antibodies against HER2 using reducitve amination methods. We use dynamic light scattering, and absorption and fluorescence spectroscopy for phyiscal characterization of the constructs. Flow cytometry and fluorescence microscopy are used to investigate molecular targeting and imaging capabilities of the constructs against SKOV3 and OVCAR3 ovarian cancer cell lines, which have relatively high and low expression levels of the HER2 receptor, respectively. Continuous NIR laser irradiation at 808 nm is used to investigating the utility of the constructs in mediating photothermal destruction of SKOV3 cells.

Results: Flow cytometry results indicate that the functionalized nano-constructs are more effective in targeting the HER2 receptor than non-encapsulated ICG and non-functionlaized constructs ($P < 0.005$). Fluorescence microscopic images show the capaiblity of the functionalized constructs in NIR imaging of HER2 over-expression. The functionalized nano-constructs are also capable of inducing a significantly greater increase in photothermal destruction of SKOV3 cells than free ICG and non-functionalized constructs ($P < 0.005$).

Conclusion: We have demonstrated the efficacy of polymeric nano-structured constructs loaded with ICG, and functionalized with the monoclonal antibodies, as thernaostic materials for targted molecular NIR imaging of the HER2 receptor overexpression on ovarian cancer cells, and photothermal destruction of these cells. These nanoparticles may prove useful towards intraoperative detection, imaging, and phototherapy of small ovarian cancer nodules. Lasers Surg. Med. 46:582–592, 2014.

Key words: cytoreduction; her2; laser therapy; nanomedicine; optical imaging; tumor

INTRODUCTION

Ovarian cancer is the deadliest gynecological cancer in women [1]. Only about 20% of ovarian cancers are diagnosed when the disease is confined to the ovaries [2] (classified as stage I [3]). Once the disease spreads beyond the ovaries, and extends into the pelvis (below the pelvic brim) (stage II), the peritoneum outside the pelvis and/or into the retroperitoneal lymph nodes (stage III), or metastasizes distantly to hepatic and/or splenic parenchymal or the extra-abdominal organs (stage IV), the survival rate is greatly diminished [2], with 5-year survival rates less than 20% [4].

Treatment of ovarian cancer is based on cytoreductive surgery, with the goal of reducing the burden of the cancer

Contract grant sponsor: Bourns College of Engineering; Contract grant sponsor: Bioengineering Center at University of California, Riverside; Contract grant sponsor: National Science Foundation; Contract grant numbers: CBET-1403191, CBET-1402353, CBET-1144237, CBET-0923408; Contract grant sponsor: American Society for Laser in Surgery and Medicine (ASLMS); Contract grant sponsor: International Society for Optics and Photonics (SPIE).

*Correspondence to: Bahman Anvari, PhD, Department of Bioengineering, University of California, Riverside, 211 Materials Science & Engineering Building, 900 University Ave., Riverside, CA 92521. E-mail: anvarib@ucr.edu

Accepted 26 May 2014
Published online 24 June 2014 in Wiley Online Library (wileyonlinelibrary.com).
DOI 10.1002/lsm.22269

to none or minimal residual tumor deposits, followed commonly by administration of standard chemotherapeutic combination of carboplatin and paclitaxel [5–7]. However, most patients suffer from recurrence, and are chemoresistant [5,7].

The degree of success in cytoreductive surgery is an important prognostic factor, with improved survival associated with complete resection of all visible cancer [8–10]. Yet, a great challenge during cytoreduction remains the detection of small (diameter <1 cm) intraperitoneal tumor deposits. The current surgical standard is to remove all visible deposits, on the order of 1–2 cm nodules. Smaller nodules are difficult to detect pre-operatively by computed tomography scans, magnetic resonance imaging, or visually at surgery, and if left behind, can result in recurrence, which is unfortunately all too common with this disease. It is both widely metastatic disease that cannot be removed at the time of surgery and the chemoresistance of ovarian cancer that results in high mortality from ovarian cancer.

Imaging methods that can identify small tumor nodules, not detectable by existing methods, offer the potential to enhance diagnosis and lead to improved therapeutic outcomes. Intraoperative fluorescence imaging based on materials that are optically activated by near infrared [NIR] wavelengths [$\approx$700–1,450 nm] provides a potentially effective approach. NIR imaging provides two key advantages: (1) due to the reduced absorption of photons by water and proteins, as well as the diminished scattering within the NIR spectral band, optical penetration depth is increased to allow identification of tumors extending to $\approx$2–3 cm in depth; and (2) given that there is minimal autofluorescence in the NIR spectral bands, the use of an exogenous chromophore enhances the imaging contrast. Intraoperative NIR fluorescence imaging, as an optical modality with high resolution ($\approx$100 μm), has gained entry into early clinical studies [11,12]. By combineing it with a molecular targeting agent, the specificity of such fluorescent probes can be enhanced.

One particular NIR imaging agent is indocyanine green [ICG]. The first medical applications of ICG date back to the late 1950s for measurements of cardiac output. The finding that ICG is almost exclusively taken up by the liver, led to its application in assessment of hepatic function. In 1975, ICG received supplemental approval by FDA for ophthalmic angiography. To-date, ICG remains the only FDA-approved NIR dye for cardiocirculatory measurements, liver function tests, and imaging of selective ophthalmological disorders including suspected polypoidal choroidal neovascularization, chronic central serous chorioretinopathy, and choroidal hemangioma. ICG has also been investigated for sentinel lymph node (SLN) mapping and staging in cancer patients [13–16]. In addition to its NIR imaging capabilities, ICG has been studied for potential phototherapeutic applications including treatment of chronic central serous chorioretinopathy [17], and cutaneous hypervascular malformations [18,19].

Despite its usage in clinical medicine, the major drawbacks of ICG are its short half-life within plasma [$\approx$2–4 minutes], and lack of targeting capability. ICG encapsulation has been investigated as a methodology to overcome these limitations [20,21]. We have reported that encapsulation of ICG into nanocapsules composed of the polymer poly(allylamine) hydrochloride (PAH) chains cross-linked ionically with sodium phosphate, and coated with polyethylene glycol (PEG), delays maximal hepatic accumulation to at least 60 minutes after tail vein injection in mice [22]. Furthermore, the reactive amines on the encapsulating shell provide a platform to attach appropriate moieties for targeted molecular imaging of a disease biomarker.

The human epidermal growth factor receptor-2 (HER2), presents an important biomarker for targeted imaging of ovarian cancer cells. HER2 is one of the four members of the HER family of transmembrane proteins (HER1, HER2, HER3, and HER4), all of which play a key role in carcinogenesis of various solid tumors, particularly breast, colorectal, non-small cell lung cancer, and ovarian cancer [23–25]. Among the four family proteins, HER2 has the strongest catalytic kinase activity, and its aberrations (gene amplification, gene mutations, and protein overexpression) are reported in diverse malignancies, including ovarian cancer [26]. The reported percentage of ovarian cancer patients with HER2 overexpression is variable, and ranges between approximately 5–52% [27–31]. According to a recent study, conventional immunohistochemical (IHC) analysis underestimates the true frequency of HER2 expressing ovarian cancers [32]. Whereas IHC analysis revealed HER2 overexpression in only 29% of high-grade ovarian serous carcinoma sites, more sensitive detection methods including flow cytometry, Western blot analysis, and quantitative-polymerase chain reaction (q-PCR) demonstrated HER2 expression in all tumor cells derived from solid tumors and primary ascites, as well as all established and short-term cultured cancer cells [32]. Importantly, HER2 overexpression is reported to have prognostic significance since increased HER2 expression has been correlated with reduced survival [31], and increased risk of progression and death [29,30].

Our nano-construct system composed of ICG-doped nanocapsules (ICG-NCs), functionalized with an antagonist against the HER2 receptor, offers a potential platform for targeted molecular imaging of an important biomarker associated with ovarian cancer. Moreover, the encapsulated ICG can potentially serve as a therapeutic agent to induce photothermal destruction of the cancer cells in response to NIR laser irradiation. Therefore, detection, imaging, and phototherapeutic capabilities can be provided by a single nano-structured NIR platform. Herein, we report the effectiveness of these nano-constructs for targeted NIR fluorescence imaging of ovarian cancer cells expressing HER2 receptors, and photothermal destruction of these cells *in vitro*.

MATERIALS AND METHODS

Reagents

Sodium phosphate dibasic heptahydrate ($Na_2HPO_4.7H_2O$, Fisher Scientific, Hampton, NH), poly(allylamine) hydrochloride (PAH, Sigma–Aldrich), indocyanine green (Sigma–

Aldrich, St. Louis, MO), methoxy-poly(ethylene glycol)-butyraldehyde (PEG-ALD, MW = 5,000 Da, Laysan Bio, Inc.), butyraldehyde-poly(ethylene glycol)-butyraldehyde (ALD-PEG-ALD, MW = 10,000 Da, Laysan Bio, Inc., Arab, AL), Sodium dithionite ($Na_2S_2O_4$, Sigma–Aldrich), phosphate buffer saline (PBS, Fisher BioReagents, Hampton, NH), and monoclonal rabbit antibody to HER-2 receptor (anti-HER2, Diagnostic Biosystems, Inc., Pleasanton, CA) were used as purchased. We used the SKOV3 (ATCC®, Manassas, VA) human ovarian cancer cell line, which is phenotypically identical to epithelial ovarian cancer cells [33], and has relatively high expression levels of the HER2 receptor [34]. As control cells, we used the OVCAR3 cell lines (ATCC®), established from the malignant ascites of human ovarian adenocarcinoma, which have relatively low expressions of the HER2 receptor [35]. Cells were cultured separately in McCoy's 5a Medium supplemented with 10% fetal bovine serum, and 1% penicillin.

ICG-NCs Synthesis and Antibody Conjugation

We have previously reported the fabrication process of ICG-NCs in details [22,36,37]. Briefly, 10 ml of disodium hydrogen phosphate heptahydrate solution (0.01 M, 4°C) and 20 ml of PAH stock solution (2 mg/ml, 4°C) were mixed in the first step. The resulting nanoparticle suspension was diluted by adding 1.2 ml pre-cooled deionized water (4°C) immediately before addition of 240 ml of ICG aqueous solution (0.65 mM, 4°C). The ICG-NC suspension was aged for 15 minutes at 4°C followed by washing through differential centrifugation described in details previously [22].

To covalently attach the anti-HER2 antibodies to the surface of the nano-constructs, we utilized our previously reported biochemical methods based on reductive amination (Fig. 1) [37,38]. Specifically, we added single-aldehyde terminated 5 kDa polyethylene glycol (PEG) and double-aldehyde terminated 10 kDa PEG polymers, in an equal ratio, to 1 ml of the ICG-NCs solution, followed by addition of 200 ng of anti-HER2. The double aldehyde-terminated PEG serves as the linker for covalent attachment to the available amines on the surface of ICG-NCs, and the amines on the antibody. The single aldehyde-terminated PEG serves to reduce non-specific protein adsorption to the surface of ICG-NCs [37]. A previous study has demonstrated that among PEG molecules with molecular weight in the range of 1–20 kDa, the use of the 5 kDa PEG provided the optimal covalently grafted coating to suppress non-specific adhesion [39].

We subsequently added 5 μl of 0.02 M sodium dithionite as the reducing agent. The suspension was gently mixed for 10 seconds and aged for 1 hour at 4°C in the dark, and then washed by centrifugation twice at 4,600*g* for 10 minutes. The pelleted ICG-NCs coated with anti-HER2 and PEGylated (referred to as anti-HER2-PEG-ICG-NCs) were resuspended in PBS and stored at 4°C in dark.

Characterization of Functionalized ICG-NCs

The hydrodynamic diameter of non-functionalized ICG-NCs and anti-HER2-PEG-ICG-NCs were measured by dynamic light scattering (DLS) (Zetasizer Nanoseries, NanoZS90, Malvern Instruments, Malvern, UK). The absorption spectra of non-functionalized ICG-NCs and anti-HER2-PEG-ICG-NCs were obtained using a UV-Visible spectrophotometer (Cary 50 UV-Vis spectrophotometer, Agilent Technologies, Santa Clara, CA) with optical pathlength of 1 cm. The fluorescence spectra of ICG-NCs, in response to 680 nm excitation with a 450 W xenon lamp, were recorded using a fluorometer (Fluorolog-3 spectrofluorometer, Edison, NJ). We obtained the normalized fluorescence spectra $\zeta(\lambda)$ as:

$$\zeta(\lambda) = \frac{F(\lambda)}{[1 - 10^{-A(\lambda_{ex})}]} \quad (1)$$

where $F(\lambda)$ is the recorded emission intensity at wavelength, λ, and $A(\lambda_{ex})$ is the absorbance value of the sample at excitation wavelength, λ_{ex}.

Flow Cytometry

A flow cytometer (FACSAria cell sorter, BD Biosciences, San Jose, CA) was used to quantify the specific targeting of

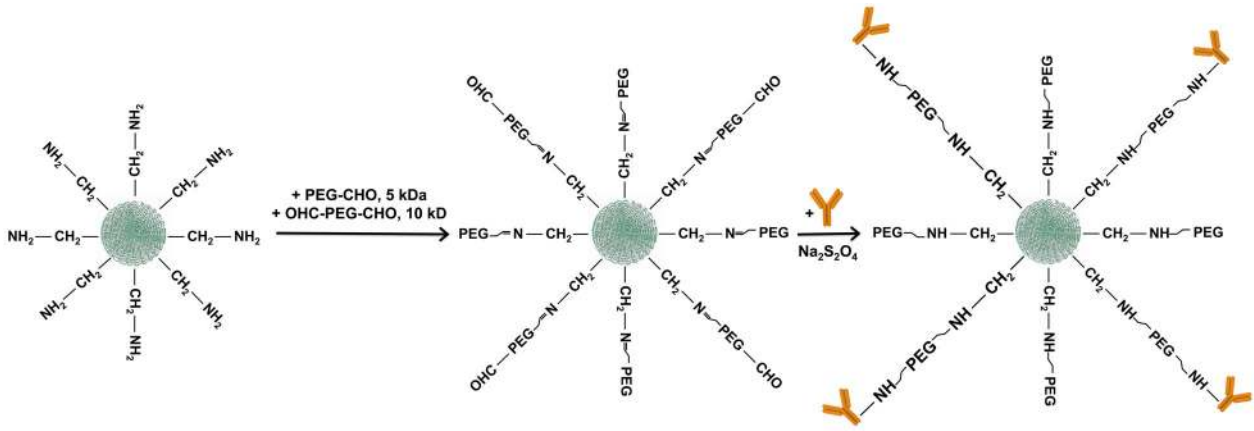

Fig. 1. Schematic for PEGylation and covalent attachment of the monoclonal antibody against the HER2 receptor.

the SKOV3 cells with anti-HER2-PEG-ICG-NCs. SKOV3 cells were cultured in 12 wells plates a night before the experiments. On the following day, the SKOV3 cells were incubated in the dark at 37°C with either free ICG, non-functionalized ICG-NCs, or anti-HER2-PEG-ICG-NCs for various time intervals ranging between 30 minutes and 3 hours, and supplied with 5% CO_2. SKOV3 cells not incubated with any of the agents were used as a negative control. Following each incubation time, cells were washed with PBS twice through centrifugation (135*g* for 4 minutes) and re-suspended in PBS. Dead cells were identified by the Propidium iodide (PI) assay, and excluded from the analysis. The prepared samples were excited at 633 nm, with emission collected at >785 nm. We define the percentage of ICG positive SKOV3 cells as the ratio of those cells emitting NIR signal to the total number of live cells.

Fluorescence Microscopy

To prepare the samples for fluorescence microscopy, 100 μl of SKOV3 or OVCAR3 cell suspension in fresh media ($\approx 10^6$ cells/ml) was added to each well of a 96-well flat-bottomed micro-titer plate. In the first set of experiments, we intentionally incubated the cells at 4°C with either free ICG, non-functionalized ICG-NCs, or anti-HER2-PEG-ICG-NCs to minimize/prevent internalization of the constructs, which normally occurs at 37°C. Cell suspensions were plated in 5% CO_2 overnight. On the following day, the old culture medium was replaced with fresh medium, and 100 μl of free ICG (10 μM, dissolved in PBS), non-functionalized ICG-NCs, or anti-HER2-PEG-ICG-NCs was added to different wells. All three agents had the same absorbance value (≈0.75) at 680 nm. Cells were incubated with the agents for 3 hours at 4°C in the dark, and subsequently washed twice with cold PBS. Finally, we incubated the cells with 4′,6-diamidino-2-phenylindole (DAPI) for 10 minutes to stain cell nuclei for fluorescence imaging. The fluorescence emission from DAPI in the range of 435–485 nm was collected in response to 360 ± 20 nm excitation by a Nikon Mercury/Xenon arc lamp. The NIR fluorescence emission (>770 nm) in response to 740 ± 35 nm excitation was captured using a long pass filter in conjunction with an electron multiplier CCD camera (Quant EM-CCD, C9100-14, Hamamatsu, Shizuoka-ken, Japan) with 100 milliseconds integration time.

In the second set of experiments, we evaluated the interaction of the SKOV3 cells with free ICG, non-functionalized ICG-NCs, or anti-HER2-PEG-ICG-NCs at physiological temperature (37°C). The procedure was identical to that used for 4°C incubation except that the incubation time at 37°C for the various agents was 2 hours. SKOV cells incubated at 37°C were fluorescently imaged using a confocal microscope (Pathway High Throughput Automated Imager, Atto Biosciences, Rockville, MD). The cells nuclei, labeled with DAPI, were imaged using an excitation wavelength of 350 nm excitation wavelength with fluorescence emission > 400 nm captured by a long pass filter. NIR fluorescence images were acquired for emissions >780 nm in response to 780 nm excitation. The camera exposure time was set at 1 second. We present all microscopic fluorescent images as the overlay of the NIR emission due to ICG (red channel), and visible emission due to DAPI-stained nuclei (blue channel).

Laser Irradiation

To quantify the photothermal response of anti-HER2-PEG-ICG-NCs to NIR irradiation, we irradiated 120 μl of functionalized ICG-NCs suspended in PBS at 808 nm. For comparison, we irradiated 120 μl of 17.2 μM free ICG dissolved in PBS, and non-functionalized ICG-NCs suspended in PBS. In this manner, the three agents had the same absorbance value (≈0.8) at 808 nm. We irradiated 120 μl of PBS as the negative control. For all samples, the irradiated spot diameter (d_o), irradiance (I_o), and irradiation time (Δt_{laser}) were 2.2 mm, 19.7 W/cm^2, and 180 seconds, respectively. Temperature during irradiation of each sample was measured using a negative temperature coefficient thermistor (20 kV, Vernier), placed 2 mm outside the irradiation spot, and connected to a Vernier LabQuest.

To investigate the photo-destructive capability of anti-HER2-PEG-ICG-NCs, we cultured SKOV3 cells in 96-well-plates over night to yield cell density of $\approx 10^6$ cells/ml. On the following day, cells were incubated with either 17.2 μM free ICG dissolved in PBS, non-functionalized ICG-NCs, or anti-HER2-PEG-ICG-NCs (latter two suspended in PBS) in separate wells for 3 hours in dark at 37°C supplied with 5% CO_2. When applied at the volume of 12.5 μl, all three agents had the same absorbance value (≈0.8) at 808 nm. We also performed experiments where we added increasing volumes (25, 50, 100, and 200 μl) of the solution of each agent to the cells. In the case of free ICG, effectively larger amounts of ICG were applied with increased volumes since we maintained the same ICG concentration (17.2 μM) in all volumes. We expect that in the cases of ICG-NCs and anti-HER2-PEG-ICG-NCs, increasing the applied volume from 12.5 to 200 μl effectively increased the number of particles by ≈16 times. Cells were then washed twice with PBS prior to laser irradiation experiments. SKOV3 cells incubated with PBS were irradiated as negative control. Each well was irradiated at two different spots ($d_o = 2.2$ mm) using an 808 nm laser wavelength with $\Delta t_{laser} = 200$ seconds, and $I_o = 19.7$ W/cm^2. Following laser irradiation, cells were stored for 2 hours at 37°C supplied with 5% CO_2. Cell viability in each well was analyzed using a live/dead assessment kit for mammalian cells (L3224, Invitrogen, Carlsbad, CA) and a fluorescent microplate reader (Molecular Devices FlexStation II 384, Harlow Scientific, Arlington, MA). Specifically, live cells were identified using Calcein ($\lambda_{excitation} = 494$ nm, peak $\lambda_{emission} = 517$ nm), and dead cells by Ethidium homodimer-1 ($\lambda_{excitation} = 528$ nm and peak $\lambda_{emission} = 617$ nm) staining.

RESULTS

The estimated peak diameter of non-functionalized ICG-NCs and anti-HER2-PEG-ICG-NCs were 58 and 102 nm,

respectively (Fig. 2A). Thus, the thickness of the coating composed of mixed 5 kDa PEGs, and 10 kDa PEGs as linkers for attachment of anti-HER2, was about 22 nm. The absorption spectrum of anti-HER2-PEG-ICG-NCs suspended in PBS was nearly identical to that of non-functionalized ICG except in the range <309 nm (Fig. 2B), indicating the successful grafting of the antibodies to the surface of the nano-constructs. The anti-HER2-PEG-ICG-NCs also retained their fluorescence capability (Fig. 2C).

As determined by flow cytometry, the population distributions of SKOV3 cells incubated with anti-HER2-PEG-ICG-NCs demonstrated a shift to the right (higher ICG fluorescent signal) as incubation time increased from 30 minutes to 3 hours at 37°C (Fig. 3A–D). Moreover, at all incubation times, notably larger population of SKOV3 cells were detected in ICG fluorescent channel. The population distributions of SKOV3 cells incubated with free ICG and non-functionalized ICG-NCs, detected in ICG channel, were very close to the negative control (SKOV3 cells incubated only in culture medium without any NIR reagents) at 30 minutes and 1-hour post-incubation. The number of cells detected in ICG channel increased for 2 and 3 hours of incubation times with non-functionalized ICG-NCs, but still remained low for cells incubated with free ICG.

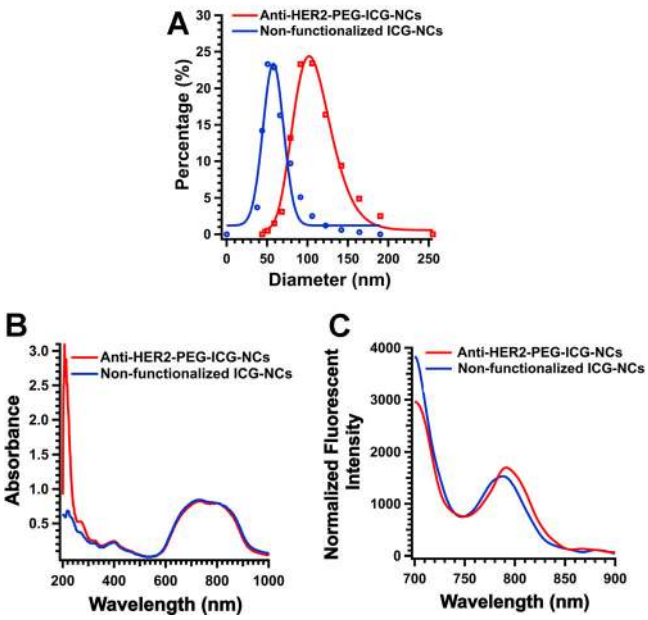

Fig. 2. **A**: Hydrodynamic diameter distribution of non-functionalized ICG-NCs and anti-HER2-PEG-ICG-NCs measured by dynamic light scattering. Circles and squares present mean of three different measurements. The curves are fitted Gaussian and Lognormal functions to the measured distributions associated with non-functionalized ICG-NCs and anti-HER2-PEG-ICG-NCs, respectively. **B**: Absorption spectra of non-functionalized ICG-NCs and anti-HER2-PEG-ICG-NCs. **C**: Normalized fluorescence spectra of non-functionalized ICG-NCs and anti-HER2 functionalized ICG-NCs in response to 680 nm photo-excitation. Emission spectra were smoothed using IGOR Pro software with second order binominal algorithm.

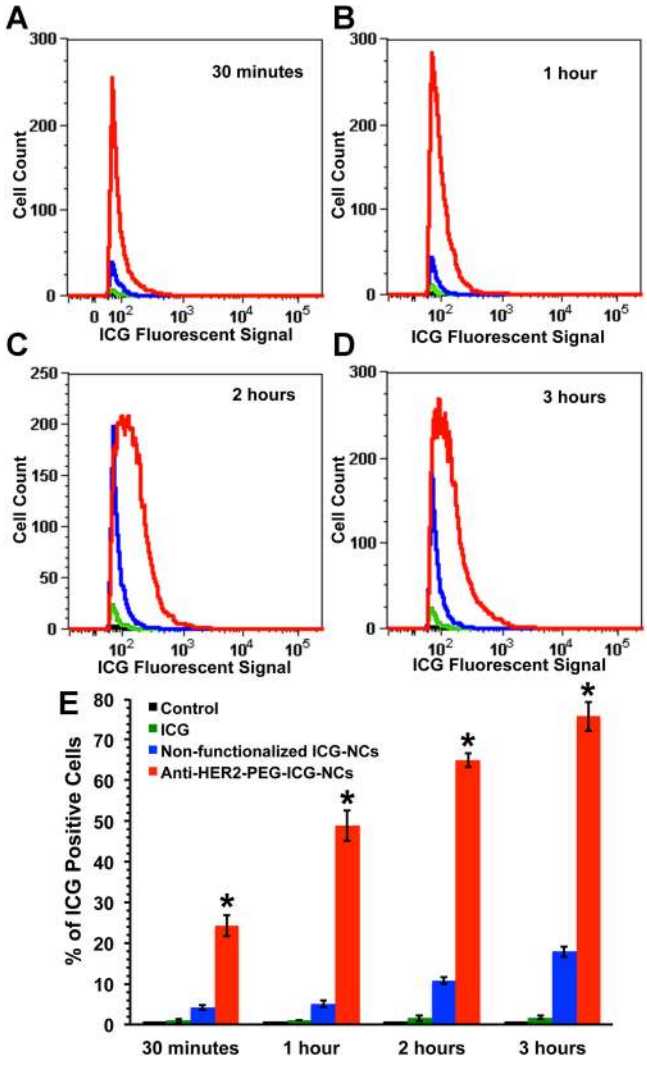

Fig. 3. Population distribution of SKOV3 cancer cells incubated with free ICG (positive control) (green), non-functionalized ICG-NCs (blue), anti-HER2-PEG-ICG-NCs (red), and McCoy's 5a culture medium containing none of the optical reagents (negative control) (black) for (**A**) 30 minutes, (**B**) 1 hour, (**C**) 2 hours, and (**D**) 3 hours at 37°C. **E**: Percentage of ICG positive cells after incubation with free ICG (positive control), non-functionalized ICG-NCs, anti-HER2-PEG-ICG-NCs, and no optical reagents (negative control) for 30 minutes, 1, 2, and 3 hours. Each bar represent mean of measurement in three different samples. Error bars are presenting single standard deviation. Asterisks denote statistically significant difference between the percentage of ICG positive cells incubated with anti-HER2-PEG-ICG-NCs, and those cells incubated with the free ICG, non-functionalized ICG-NCs, or no optical agents ($P < 0.005$, two-tailed t-test).

The fraction of ICG positive SKOV3 cells was significantly higher for those incubated with anti-HER2-PEG-ICG-NCs, and became progressively larger with increased incubation time (Fig. 3E). For example, at 3 hours of incubation time, approximately 76% of the SKOV cells incubated with anti-HER2-PEG-ICG-NCs were ICG positive, nearly four times higher than those cells incubated with non-functionalized ICG-NCs.

The highly specific molecular targeting of the HER2 receptor was further validated by fluorescence imaging of cells incubated with anti-HER2-PEG-ICG-NCs at 4°C for 3 hours (Fig. 4). The overlay of the NIR and visible fluorescent images of the SKOV3 cells incubated with anti-HER2-PEG-ICG-NCs showed the localization of the functionalized particles on the SKOV3 cell membrane as the red ring. The OVCAR3 cells, and SKOV3 cells incubated with free ICG or non-functionalized ICG showed none or minimal NIR signal. These results suggest that the interaction of anti-HER2-PEG-ICG-NCs with SKOV3 cells was highly specific and receptor-mediated.

We present confocal fluorescent images of SKOV3 cells after 2 hours of incubation with freely dissolved ICG, non-functionalized ICG-NCs, and anti-HER2-PEG-ICG-NCs at physiological temperature (37°C) (Fig. 5). NIR emission was detected from SKOV3 cells incubated with anti-HER2-PEG-ICG-NCs, and the constructs appeared to be localized to the peripheries of the cell nuclei. There was no or minimal NIR emission from the SKOV3 cells incubated with freely dissolved ICG, or non-functionalized ICG-NCs. These results confirm that specific targeting of SKOV3 cells at physiological temperatures can be achieved by anti-HER2-PEG-ICG-NCs.

The photothermal responses of ICG-NCs with and without surface functionalization were similar to that of free ICG under the same irradiation conditions ($\lambda = 808$ nm, $d_o = 2.2$ mm, $\Delta t_{laser} = 180$ seconds, and $I_o = 19.7$ W/cm^2) (Fig. 6A), indicating that encapsulation did not compromise the heat generating capability of ICG. Respective temperature rises to maximum values of ≈50, 52, and 52°C, from the baseline temperature of 20°C, during the first 100 seconds of irradiation of free ICG, non-functionalized ICG-NCs, and anti-HER2-PEG-ICG-NCs, were followed by reductions in temperature. These temperature measurements represent the lower bound estimates of the actual temperature rises of the three agents since they were made at a distance of 2 mm away from the irradiated spot. We attribute the reduction in temperature with sustained laser irradiation to thermally-induced degradation in optical absorption properties of ICG [40].

The live/dead assay confirmed that in response to laser irradiation ($\lambda = 808$ nm, $d_o = 2.2$ mm, $\Delta t_{laser} = 200$ seconds, and $I_o = 19.7$ W/cm^2) fractions of SKOV3 cell death were significantly greater ($P < 0.005$) with HER2-PEG-ICG-NCs than those induced by free ICG, or non-functionalized ICG-NCs at all investigated volume levels (Fig. 6B), indicating that anti-HER2-PEG-ICG-NCs were effective in photothermal destruction of SKOV3 cells. For example, when applied at 200 μl, anti-HER2-PEG-ICG-NCs were able to induce nearly 86% cell death.

DISCUSSION

We have previously demonstrated the utility of non-functionalized IC-NCs for *in vivo* NIR fluorescence imaging in healthy mice [22,41], and investigated their heat generation capability in tumor-simulating phantoms [42]. We have also determined that only about 5% of ICG is released from the capsules after 1 hour of incubating the

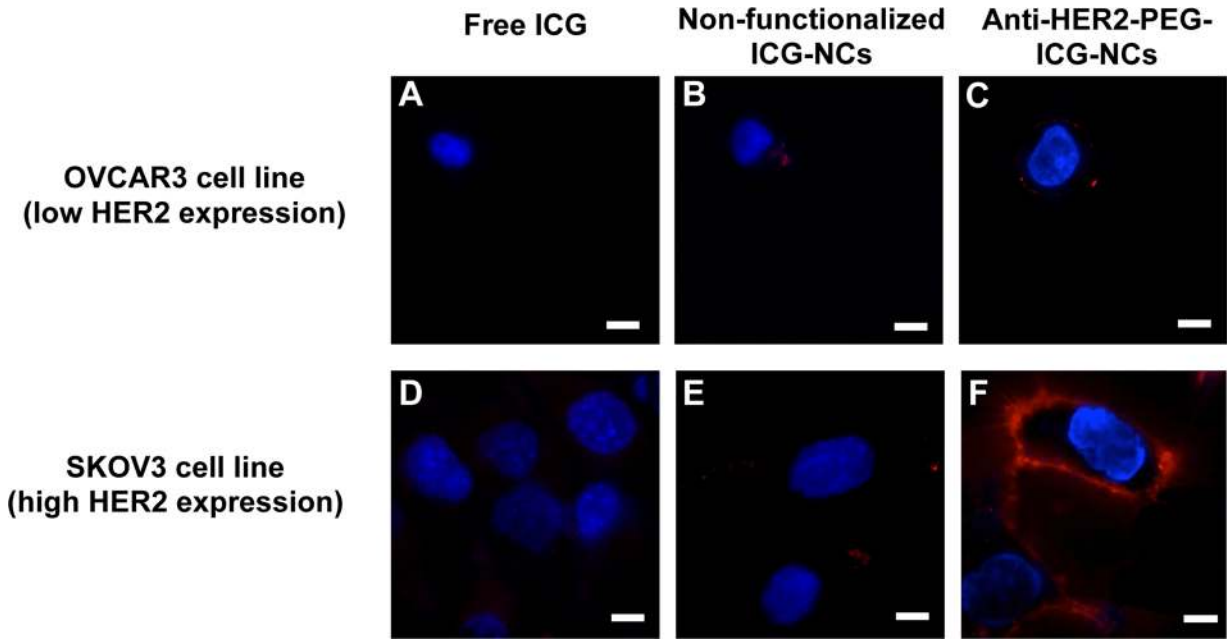

Fig. 4. Fluorescent images of OVCAR3 (panels **A**–**C**) and SKOV3 (panels **D**–**E**) cells incubated with media containing freely dissolved ICG in PBS (A, D), non-functionalized ICG-NCs (B, E), and anti-HER2-PEG- ICG-NCs (C, **F**) at 4°C for 3 hours. Cell nuclei were stained by DAPI, and falsely colored in blue using ImageJ software. The NIR fluorescent signal from ICG was falsely colored in red. Scale bars correspond to 10 μm.

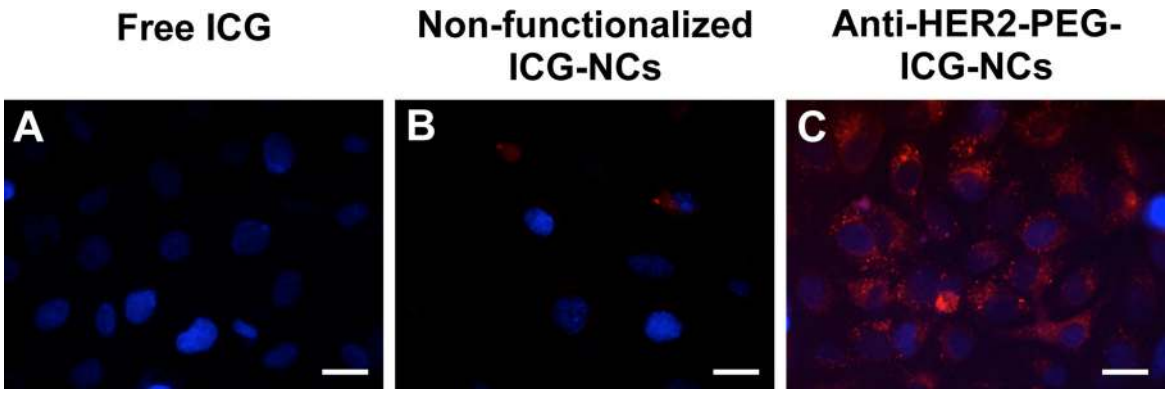

Fig. 5. False-colored confocal fluorescent images of SKOV3 cells incubated with media containing (**A**) freely dissolved ICG in PBS, (**B**) non-functionalized ICG-NCs, and (**C**) anti-HER2-PEG-ICG-NCs at 37°C for 2 hours. Cells nuclei were stained by DAPI, and falsely colored in blue using ImageJ software. The NIR fluorescent signal from ICG was falsely colored in red. Scale bars correspond to 20 μm.

constructs in Dulbecco's Modified Eagle Medium supplemented with 10% fetal bovine serum at 37°C, with the released fraction approaching a steady value of ≈8% after 24 hours [43]. The present study is the first demonstration of the use of these constructs, conjugated at their surface with covalent attachment of PEG and anti-HER2, and using ICG as the single chromophore for both NIR fluorescence imaging and photothermal destruction of ovarian cancer cells.

The estimated coating thickness on the surface of the constructs is about 22 nm. Upadhyayula et al. [39] have measured the average thickness of PEG layers with molecular weights, in the range of 1–20 kDa, grafted on flat surfaces using spectroscopic elipsometry. They

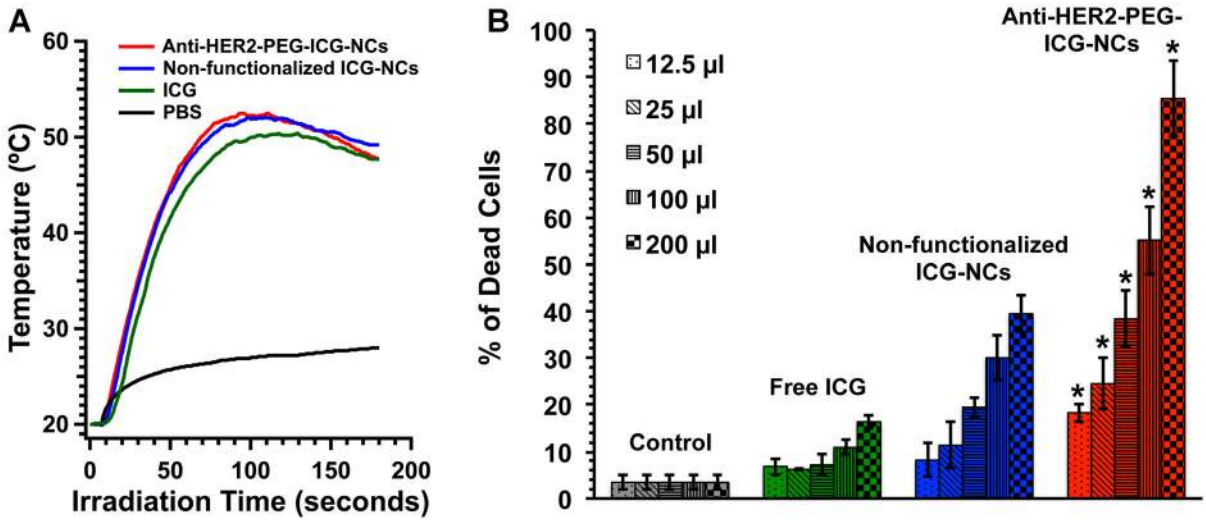

Fig. 6. **A**: Photothermal response of 120 μl of 17.2 μM free ICG dissolved in PBS, non-functionalized ICGNCs, anti-HER2-PEG-ICG-NCs suspended in PBS, and PBS solution (negative control) in response to continuous 808 nm laser irradiation with $d_o = 2.2$ mm, $\Delta t_{laser} = 180$ seconds, and $I_o = 19.7\,W/cm^2$. Temperature measurements were made 2 mm away from the irradiated spot. **B**: Percentage of dead ovarian cancer cells (SKOV3) in response to continuous 808 nm laser irradiation with $d_o = 2.2$ mm, $\Delta t_{laser} = 200$ seconds, and $I_o = 19.7\,W/cm^2$. Two different spots were irradiated in each sample. Cells were incubated with five different volumes of free ICG (17.2 μM), non-functionalized ICG-NCs, or anti-HER2-ICG-NCs functionalized ICG-NCs for 3 hours. SKOV3 cells incubated with PBS were used as negative control. Bars represent mean of three different samples, and error bars are the standard deviations. Asterisks denote statistically significant differences in cell death between those incubated with anti-HER2-PEG-ICG-NCs at a given volume, and those incubated with the other agents at the corresponding volume ($P < 0.005$, two-tailed t-test).

estimated the thicknesses of the 5 and 10 kDa PEG layers as 23 and 33 nm, respectively. The coating of the NCs appears to be closer to the 5 kDa, which we can attribute to several factors: (1) the 5 kDa PEG chains dominate the packing while the 10 kDa PEGs could be bent and even loop to bind to the particles via their two termini; (2) compared to flat surfaces, the large curvature of the NCs may contribute to decrease in the thickness of the coating because of a decrease in the packing density toward the exterior of the layer; and (3) the antibody, that has dimensions in the order of 10 nm in length does not contribute to the effective thickness of the coating as measured by DLS.

We attribute the absorption peak of the anti-HER2-PEG-ICG-NCs at 270 nm (Fig. 2B) to electronic transitions in amino acids such as tryptophan and tyrosine associated with the antibody. The NIR absorption band in 730–810 spectral range is attributed to the ICG. In comparison to free ICG dissolved in PBS at diluted concentrations (e.g., $\approx$3 μM), which has a distinct spectral peak at 780 nm (associated with monomeric form of ICG [40]), ICG-NCs have nearly uniform absorbance values in the 730–810 nm spectral range. This near uniform absorption over the 730–810 nm is consistent with our previously reported spectra for non-functionalized ICG-NCs [36,37], and can be attributed to the presence of various conformational states of ICG when encapsulated, including ICG bound to PAH. In response to photo-excitation at 680 nm, these constructs exhibit NIR emissions peaks at 792 and 700 nm, which can originate from the monomer and H-like aggregate forms of ICG, respectively [44].

The effectiviness of using the non-NIR fluorescent tracer, fluorescein isothiocyanate [FITC] (with peak emission at 520 nm when photo-excited at 495 nm), conjugated with folate hapten for targeted real time optical imaging of the folate receptor-α overexpression as a biomarker, was demonstrated for the first time in women with ovarian cancer [45]. Disseminated tumor deposits within the peritonum could be visualized with resolution of $\approx$1 mm. Despite the use of non-NIR wavelengths, this study clearly demonstrated that molecularly-targeted intraoperative fluorescence imaging of intraperitoneal tumors in humans is feasible, and provides a potentially effective approach for detection of disseminated noduldes that cannot be currently identified by existing methods.

There have been several recent studies in using NIR exogenous chromophores without and with targeting moieties for fluorescent imaging of peritoneal ovarian tumors in mice [33,46–49]. While some of these studies report the feasibility of imaging sub-millimeter tumor nodules [46,47,50], combined NIR imaging and photothermal destruction of ovarian tumors were not investigated. In one study, xenografted tumor nodules as small as $\approx$300 μm could be imaged in mice peritoneal cavity at 6 and 24 hours post-administration of 100 μl of 100 mM free ICG dissolved in PBS via the tail vain [50]. Since no specific molecular biomarker were targeted in this study, the accumulation of free ICG in tumors may have been due to the enhanced permeability and retention effect [51,52], where ICG may resemble a macromolecule upon binding to serum proteins such as albumin [50].

On the phototherapeutic side, there is precedence for photodynamic therapy (PDT) of intraperitoneal tumors in humans as a non-photothermal approach that relies mainly on formation of singlet oxygen or radicals as cytotoxic agents [53–55]. In one study [54], 13 ovarian cancer patients underwent PDT using the chromophore dihematoporphyrin ethers (DHE), in conjunction with 630 nm laser irradiation, where light was delivered to mesentery and bowel by a flat-cut optical fiber. In other areas, including the pelvis, light was delivered through a diffusing wand. In another study [55], 39 patients underwent debulking surgery and PDT using DHE in conjunction with either 630 or 514 nm laser irradiation. In some patients, the entire peritoneal surface was laser irradiated. Therefore, intraoperative laser irradiation of intraperitoneal tumors in humans is also possible. Nevertheless, these studies lacked specific tumor targeting and imaging capabilities to determine the spatiotemporal distribution of the chromophore in tumors. Our results presented herein indicate that anti-HER2-PEG-ICG-NCs provide capabilities for biomarker detection, imaging, and photothermal theraphy in a single nano-structured NIR optical platform.

In a recent *in vitro* study, Mir et al. [56] demonstrated the effecacy of photo-destruction of OVCAR5 human epithelial ovarian carcinoma cells using a pre-formed commerically aviablable liposomal system. Benzoporphyrin derivative monoacid A as the PDT agent, and Cetuximab (C225) to target HER1, were passively (non-covalently) adsorbed on the surface of the liposomes [56]. The investigators showed that the combined use of PDT and C225 to inhibit HER1 activity was more effective in cell killing as compared to either PDT or C225 application alone. In comparison to our study where ICG is used as both the imaging and therapeutic agent, a second chromophore, FITC, was used to lable the C225 and quantify the cellular uptake of the construct.

The combined effects of doxorubicin (DOX), an anthracycline antibiotic chemotherapeutic agent, and ICG-mediated hyperthermia on SKOV3 cells have been investigated *in vitro* [57]. Hyperthermia, mediated by use of 5 μM free ICG, in combination with DOX achieved significantly greater cell death than DOX alone, indicating the added benefit of heating in destruction of the ovarian cancer cells. Nevertheless, ICG as applied in that study, did not have specific targeting capability, and thermal injury was likely induced by heat diffusion resulting from laser-irradiated ICG in solution as opposed to direct heating of the cells uptaking ICG.

Chen et al. [58] have demonstrated the utility of nano-complexes consisting of a silica core surrounded by a gold nanoshell, further doped with ICG and superparamagnetic iron oxide, for dual NIR and MRI, and photothermal destruction of OVCAR3 cells *in vitro*. The surface of the nano-complex was modified by attachment of streptavadin, which served as the binding site for

biotinylated anti-HER2 rabbit antibody. In contrast to these nano-complexes, ICG-NCs provide several key advantages: (1) the nanocapsules spontaneously self-assemble by electrostatically-driven cross-linking of PAH polymer with phosphate anions; (2) fabrication process is entirely based on green chemistry in aqueous media within 10–30 seconds, with entire time to dope the nanocapsules with ICG not exceeding 3 hours; and (3) the inherent presence of the amines on the surface of capsules provide addressable sites for covalent attachment of various targeting moieties including the anti-HER2 antibody, without the need for additional attachment of other molecules such as streptavadin. While this proof-of-concept study has been limited to target cells that overexpress HER2, ICG-NCs can be functionalized with other moieties to target other potential biomarkers such as the folate receptor-α, or possibly be tailored to a patient specific biomarker.

Our results demonstrate that the percentage of cell death *in vitro* is directly proportional to the volume of the PBS solution containing the anti-HER2-PEG-ICG-NCs, or effectively the number of these nanoparticles (Fig. 6B). Whereas nearly 86% cell death occurred in response to application of 200 μl of solution, it is quite reasonable to expect that the *in vitro* percentage of cell death can increase further and approach 100% by increasing the solution volume (number of particles). Secondly, the percentages of cell death in this study were in response to I_o value of 19.7 W/cm^2. Increased levels of I_o should results in greater percentage of cell death *in vitro*. Therefore, by optimal combinations of solution volume (number of particles) and I_o, 100% cell death can possibly be achieved *in vitro*. Thirdly, two spots were irradiated in each well, leaving those cells close to the wall of the wells non-irradiated. In view of using non-optimal solution volume (particles number) and I_o, and despite not capturing all the cells in the wells for irradiation, we were still able to achieve 86% cell death *in vitro* by using anti-HER2-PEG-ICG-NCs.

While in this study, photothermal destruction of SKOV3 cells was achieved by inducing temperature elevations above 50°C, it may also be possible to induce cell death by laser-induced hyperthermic effects involving lower temperature increases maintained over longer irradiation times. For example, it has been indicated that almost 100% of colon adenocarcinoma cell lines could be destroyed when they were maintained at temperature of 45°C for about 40 minutes [59]. Our future work will include studies aimed at investigating the effectiveness of anti-HER2-PEG-ICG-NCs as theranostic agents for fluorescence imaging and photothermal destruction of ovarian tumors in animal models, and optimizing the laser irradiation parameters and the number of anti-HER2-PEG-ICG-NCs.

CONCLUSION

We have carried out an *in vitro* study that demonstrates the effectiveness of an optical nano-platform, consisting of the NIR chromophore ICG encapsulated within a polymer-based structure with covalently attached antibodies at the surface, for targeted molecular fluorescence imaging of the HER2 receptor as an ovarian cancer biomarker, and photothermal destruction of ovarian cancer cells expressing this biomarker. These constructs may provide the capability for intraoperative detection, imaging, and phototherapy of small ovarian cancer nodules in conjunction with open surgical procedures associated with clinical management of ovarian cancer.

ACKNOWLEDGMENTS

This study was supported in parts by the Bourns College of Engineering, the Bioengineering Center at University of California, Riverside, grants by the National Science Foundation (CBET-1403191, CBET-1402353, CBET-1144237, CBET-0923408), a student summer research grant from American Society for Laser in Surgery and Medicine (ASLMS), and a student scholarship in Optics and Photonics from International Society for Optics and Photonics (SPIE).

REFERENCES

1. Holschneider CH, Berek JS. Ovarian cancer: Epidemiology, biology, and prognostic factors. Semin Surg Oncol 2000;19:3–10.
2. Bast RC Jr, Hennessy B, Mills GB. The biology of ovarian cancer: New opportunities for translation. Nat Rev Cancer 2009;9:415–428.
3. Prat J. Staging classification for cancer of the ovary, fallopian tube, and peritoneum. Int J Gynaecol Obstet 2014;124:1–5.
4. Heintz AP, Odicino F, Maisonneuve P, Quinn MA, Benedet JL, Creasman WT, Ngan HY, Pecorelli S, Beller U. Carcinoma of the ovary. FIGO 26th Annual Report on the results of treatment in gynecological cancer. Int J Gynaecol Obstet 2006;96(Suppl 1):S161–S192.
5. Williams TI, Toups KL, Saggese DA, Kalli KR, Cilby WA, Muddiman DC. Epithelial ovarian cancer: Disease etiology, treatment, detection, and investigational gene, metabolite, and protein biomarkers. J Proteome Res 2007;6:2936–2962.
6. Metzger-Filho O, Moulin C, D'Hondt V. First-line systemic treatment of ovarian cancer: A critical review of available evidence and expectations for future directions. Curr Opin Oncol 2010;22:513–520.
7. Liu J, Matulonis UA. New advances in ovarian cancer. Oncology 2010;24:721–728.
8. Zivanovic O, Aldini A, Carlson JW, Chi DS. Advanced cytoreductive surger: American perspective. Gynecol Oncol 2009;114(2 Suppl):S3–S9.
9. Vergote I, van Gorp T, Amant F, Leunen K, Neven P, Berteloot P. Timing of debulking surgery in advanced ovarian cancer. Int J Gynecol Cancer 2008;18(Suppl 1):11–19.
10. Zhong W, Celli JP, Mai Z, Spring BQ, Yun SH, Hasan T. In vivo high-resolution fluorescence microendoscopy for ovarian cancer detection and treatment monitoring. Br J Cancer 2009;101:2015–2022.
11. Troyan SL, Kianzad V, Gibbs-Strauss SL, Gioux S, Matsui A, Oketokoun R, Ngo L, Khamene A, Azar F, Frangioni JV. The FLARE intraoperative near-infrared fluorescence imaging system: A first-in-human clinical trial in breast cancer sentinel lymph node mapping. Ann Surg Oncol 2009;16:2943–2952.
12. Vahrmeijer AL, Hutteman M, van der Vorst JR, van de Velde CJH, Frangioni JV. Image-guided cancer surgery using near-infrared fluorescence. Nat Rev Clin Oncol 2013;10:507–518.
13. Kitai T, Inomoto T, Miwi M, Shikayama T. Fluorescence navigation with indocyanine green for detecting sentinel lymph nodes in breast cancer. Breast Cancer 2005;12:211–215.
14. Sevick-Muraca EM, Sharma R, Rasmussen JC, Marshall MV, Wendt JA, Pham HQ, Bonefas E, Houston JP, Sampath L,

Adams KE, Blanchard DK, Fisher RE, Chiang SB, Elledge R, Mawad ME. Imaging of lymph flow in breast cancer patients after microdose administration of a near-infrared fluorophore: Feasibility study. Radiology 2008;246:731–741.
15. Hirche C, Murawa D, Mohr Z, Kneif S, Hunerbein M. ICG fluorescence-guided sentinel lymph node biopsy for axillary nodal staging in breast cancer. Breast Cancer Res Treat 2010;121:373–378.
16. van der Vorst JR, Schaafsma BE, Verbeek FP, Swijnenburg RJ, Hutteman M, Liefers GJ, van de Velde CJ, Frangioni JV, Vahrmeijer AL. Dose optimization for near-infrared fluorescence sentinel lymph node mapping in patients with melanoma. Br J Dermatol 2013;168:93–98.
17. Costa RA, Scapucin L, Moracs NS, Calucci D, Melo LA, Cardillo JA, Farah ME. Indocyanine green-mediated photothrombosis as a new technique of treatment for persistent central serous chorioretinopathy. Curr Eye Res 2002;25:287–297.
18. Klein A, Szeimies RM, Baumler W, Zeman F, Schreml S, Hohenleutner U, Landthaler M, Koller M, Babilas P. Indocyanine green-augmented diode laser treatment of port-wine stains: Clinical and histological evidence for a new treatment option from a randomized controlled trial. Br J Dermatol 2012;167:333–342.
19. Klein A, Baumler H, Buschmann M, Landthaler M, Babilas P. A randomized controlled trial to optimize indocyanine green-augmented diode laser therapy of capillary malformations. Lasers Surg Med 2013;45:216–224.
20. Wu L, Fang S, Shi S, Deng J, Liu B, Cai L. Hybrid polypeptide micelles loading indocyanine green for tumor imaging and photothermal effect study. Biomacromolecules 2013;14:3027–3033.
21. Yoon HK, Ray A, Lee YE, Kim G, Wang X, Kopelman R. Polymer-protein hydrogel nanomatrix for stabilization of indocyanine green towards targeted fluorescence and photoacoustic bio-imaging. J Mater Chem B Mater Biol Med 2013;1:5611–5619.
22. Bahmani B, Lytle CY, Walker AM, Gupta S, Vullev V, Anvari B. Effects of nano-encapsulation and PEGylation on biodistribution of indocyanine green in healthy mice: Quantitative fluorescence imaging and analysis of organs. Int J Nanomed 2013;8:1609–1620.
23. Steffensen KD, Waldstrom M, Andersen RF, Olsen DA, Jeppesen U, Knudsen HJ, Brandslund I, Jackobsen A. Protein levels and gene expressions of the epidermal growth factor receptors, HER1, HER2, HER3 and HER4 in benign and malignant ovarian tumors. Int J Oncol 2008;33:195–204.
24. Barthelemy J, Leblanc J, Goldbarg V, Wendling F, Kurtz J-E. Pertuzumab: Development beyond breast cancer. Anticancer Res 2014;34:1483–1492.
25. English DP, Roque DM, Santin AD. HER2 expression beyond breast cancer: Therapeutic implications for gynecologic malignancies. Mol Diagn Ther 2013;17:85–99.
26. Yan M, Parker BA, Schwab R, Kurzrock R. HER2 aberrations in cancer: Implicatinos for therapy. Cancer Treat Rev 2014; S0305-7372 (14)00043-7: doi: 10.1016/j.ctrv.2014.1002.1008:
27. Lee CH, Huntsman DG, Cheang MC, Parker RL, Brown L, Hoskins P, Miller D, Gilks CB. Assessment of Her-1, Her-2, And Her-3 expression and Her-2 amplification in advanced stage ovarian carcinoma. Int J Gynaecol Pathol 2005;24:147–152.
28. Bookman MA, Darcy KM, Clarke-Pearson D, Boothby RA, Horowitz IR. Evaluation of monoclonal humanized anti-HER2 antibody, trastuzumab, in patients with recurrent or refractory ovarian or primary peritoneal carcinoma with overexpression of HER2: A phase II trial of the Gynecologic Oncology Group. J Clin Oncol 2003;21:283–290.
29. Verri E, Guglielimini P, Puntoni M, Predelli L, Papadia A, Lorenz P, Rubagotti A, Ragni N, Boccardo F. HER2/neu oncoprotein overexpression in epithelial ovarian cancer: Evaluation of its prevalence and prognostic significance. Clinical study. Oncology 2005;68:154–161.
30. Nielsen JS, Jakobsen E, Hølund B, Bertelsen K, Jacobsen A. Prognostic significance of p53, Her-2, and EGFR overexpression in borderline and epithelial ovarian cancer. Int J Gynecol Cancer 2004;14:1088–1096.
31. Høgdall EVS, Christensen L, Kjaer SK, Blaakaer J, Bock JE, Glud E, Nørgaard-Pedersen B, Høgdall CK. Distribution of HER-2 overexpression in ovarian carcinoma tissue and its prognostic value in patients with ovarian carcinoma. Cancer 2003;98:66–73.
32. Lanitis E, Dangaj D, Hagemann IS, Song D-G, Best A, Sandaltzopoulos R, Coukos G, Powell DJ Jr. Primary human ovarian epithelial cancer cells broadly express HER2 at immunologically-detectable levels. PLoS ONE 2012;7:e49829.
33. Aina OH, Marik J, Gandour-Edwards R, Kam KS. Near-infrared optical imaging of ovarian cancer xenografts with novel alpha 3-integrin binding peptide "OA02". Mol Imaging 2005;4:437–439.
34. Tolmachev F, Wallberg H, Sandstrom M, Hansson M, Wennborg A, Orlova A. Optimal specific radioactivity of anti-HER2 Affibody molecules enables discrimination between xenografts with high and low HER2 expression levels. Eur J Nuc Mol Imaging 2010;38:531–539.
35. Delord JP, Allal C, Canal M, Mery E, Rochiax P, Hennebelle I, Pradines A, Chatelut E, Bugat R, Guichard S, Canal P. Selective inhibition of HER2 inhibits AKT signal transduction and prolongs disease-free survival in a micrometastasis model of ovarian carcinoma. Ann Oncol 2005;16:1889–1897.
36. Yu J, Javier D, Yaseen MA, Nitin N, Richards-Kortum R, Anvari B, Wong MS. Self-assembly synthesis, tumor cell targeting, and photothermal capabilities of antibody-coated indocyanine green nanocapsules. J Am Chem Soc 2010;132: 1929–1938.
37. Bahmani B, Gupta S, Upadhyayula S, Vullev VI, Anvari B. Effect of polyethylene glycol coatings on uptake of indocyanine green loaded nanocapsules by human spleen macrophages in vitro. J Biomed Opt 2011;16:051303.
38. Bahmani B, Vullev V, Anvari B. Development of ant-HER2 conjugated ICG-loaded polymeric nanoparticles for targeted optical imaging of ovarian cancer. Reporters, markers, dyes, nanoparticles, and molecular probes for biomedical applications IV; 2012; San Francisco, CA. SPIE 8233:1–6.
39. Upadhyayula S, Quinata T, Bishop S, Gupta S, Johnson NR, Bahmani B, Bozhiov K, Stubbs J, Jreij P, Nallagatle P, Vullev VI. Coatings of polyethylene glycol for suppressing adhesion between solid microspheres and flat surfaces. Langmuir 2012;28:5059–5069.
40. Bahmani B, Bacon D, Anvari B. Erythrocyte-derived phototheranostic agents: Hybrid nano-vesicles containing indocyanine green for near infrared imaging and therapeutic applications. Sci Rep 2013;3:2180. doi: 2110.1038/srep02180.
41. Yaseen MA, Yu J, Wong MS, Anvari B. In-vivo fluorescence imaging of mammalian organs using charge-assembled mesocapsule constructs containing indocyanine green. Opt Express 2008;16:20577–20587.
42. Yaseen MA, Yu J, Wong MS, Anvari B. Laser-induced heating of dextran-coated mesocapsules containing indocyanine green. Biotechnol Prog 2007;23:1431–1440.
43. Yaseen MA, Yu J, Jung BS, Wong MS, Anvari B. Biodistribution of encapsulated indocyanine green in healthy mice. Mol Pharm 2009;6:1321–1332.
44. Jung B, Vullev V, Anvari B. Revisiting indocyanine green: Effects of serum and physiological temperature on absorption and fluorescence characteristics. IEEE J Sel Top Quant 2014; 20:7000409.
45. van Dam GM, Themelis G, Crane LM, Harlaar NJ, Pleijhuis RG, Kelder W, Sarantopoulos A, de Jong JS, Arts HJ, van der Zee AG, Bart J, Low PS, Ntziachristos V. Intraoperative tumor-specific fluorescence imaging in ovarian cancer by folate receptor-α targeting: First in-human results. Nat Med 2011;17:1315–1319.
46. van Scheltinga AGT, van Dam GM, Nagengast WB, Ntziachristos V, Hollema H, Herek JL, Schroder CP, Kosterink JGW, Lub-de Hoog MN, de Vries EGE. Intraoperative near-infrared fluorescence tumor imaging with vascular endothelial growth factor and human epidermal growth factor receptor 2 targeting antibodies. J Nucl Med 2011;52:1778–1785.
47. Alexander VM, Sano K, Yu Z, Nakajima T, Choyke PL, Ptaszek M, Kobayashi H. Galactosyl human serum albumin-NMP1 conjugate: A near infrared [NIR]-activatable

fluorescence imaging agent to detect peritoneal ovarian cancer metastases. Bioconjug Chem 2012;23:1671–1679.
48. Corbin IR, Ng KK, Ding L, Jurisicova A, Zheng G. Near-infrared fluorescent imaging of metastatic ovarian cancer using folate receptor-targeted high-density lipoprotein nanocarriers. Nanomedicine [Lond] 2013;8:875–890.
49. Harlaar NJ, Kelder W, Sarantopoulos A, Bart J, Themelis G, van Dam GM, Ntziachristos V. Real-time near infrared fluorescence [NIRF] intra-operative imaging in ovarian cancer using an αvβ3-integrin targeted agent. Gynecol Oncol 2013;128:590–595.
50. Kosaka N, Mitsunaga M, Longmire MR, Choyke PL, Kobayashi H. Near infrared fluorescence-guided real-time endoscopic detection of peritoneal ovarian cancer nodules using intravenously injected indocyanine green. Int J Cancer 2011;29:1671–1677.
51. Matsumura Y, Maeda H. A new concept for macromolecular therapeutics in cancer chemotherapy: Mechanism of tumoritropic accumulation of proteins and the antitumor agent smancs. Cancer Res 1986;46:6387–6392.
52. Torchilin V. Tumor delivery of macromolecular drugs based on the EPR effect. Adv Drug Deliv Rev 2011;63:131–135.
53. Lele SB, Piver MS, Mang TS, Dougherty TJ, Tomzak MJ. Photodynamic therapy in gynecologic malignancies. Gynecol Oncol 1989;34:350–352.
54. Sindelar WF, DeLaney TF, Tochner Z, Thomas GF, Dachowski LJ, Smith PD, Friauf WS, Cole JW, Glatstein E. Technique of photodynamic therapy for disseminated intraperitoneal malignant neoplasms phase I study. Arch Surg 1991;126:318–324.
55. DeLaney TF, Sindelar WF, Tochner Z, Smith PD, Friauf WS, Thomas G, Dachowski L, Cole JW, Steinberg SM, Glatstein E. Phase I study of debulking surgery and photodynamic therapy for disseminated intraperitoneal tumors. Int J Radiat Oncol Biol Phys 1993;15:445–457.
56. Mir Y, Erlington SA, Hasan T. A new nanoconstruct for epidermal growth factor receptor-targeted photo-immunotherapy of ovarian cancer. Nanomedicine: NBM 2013;9:1114–1122.
57. Tang Y, McGoron AJ. Combined effects of laser-ICG photothermotherapy and doxorubicin chemotherapy on ovarian cancer cells. J Photochem Photobiol B 2009;97:138–144.
58. Chen W, Bardhan R, Bartles M, Perez-Torres C, Pautler RG, Halas NJ, Joshi A. A molecularly targeted theranostic probe for ovarian cancer. Mol Cancer Ther 2010;9:1028–1038.
59. Hilderbrandt B, Wust P, Alhers O, Dieing A, Sreenivasa G, Kerner T, Felix R, Riess H. The cellular and molecular basis of hyperthermia. Crit Rev Oncol Hematol 2002;43:33–56.